2024 European Control Conference (ECC)
June 25-28, 2024. Stockholm, Sweden

Modified Lyapunov Vector Fields Based Approach Plane Constrained Spacecraft Docking Guidance for Non-cooperative Tumbling Targets

Atharva Sunder Ramdas[1], Ishfaq Zahoor Bhat[2] and Debasish Ghose[3]

Abstract— **Space debris removal and on-orbit servicing missions require docking spacecraft guidance that not only enables reaching the target spacecraft but also avoids collisions with appendages protruding from it. In this paper, two modified guidance laws are proposed for spacecraft docking on non-cooperative tumbling targets, with collision avoidance, using Lyapunov Vector Fields. In the literature, a two-stage thrust-constrained guidance strategy has been proposed, with the first stage used for a station-keeping approach trajectory and the second for contraction towards the docking port. Our proposed strategy follows a similar approach but additionally ensures that the chaser spacecraft enters and stays on a safe approach plane during both stages so that collisions with protruding appendages of the target spacecraft can be avoided. This is done by introducing a third component of motion in the target's body frame away from the initial approach plane, towards a plane free from intersections with undesirable appendages. It is shown that with these modified guidance laws, asymptotic convergence is guaranteed to the respective goal locations of each stage. A maneuver design example, along with numerical simulations, is presented to demonstrate the effectiveness of the proposed guidance strategy on a real mission.**

I. INTRODUCTION

With several thousands of tumbling debris and orbiting satellites around the Earth, space agencies are recognizing the need to free up occupied low Earth orbits from space debris, especially due to the potential exponential growth of their population through collisions [1]. Studies by the European Space Agency [2] have shown that this exponential growth rate could be controlled by strategically removing five to ten large pieces of debris every year as of 2013. Considering the high costs of space travel and the growing debris population, it is essential to look into the intricacies of a debris removal mission for prompt implementation.

An early phase of such a mission is docking onto these tumbling objects. Such a maneuver would involve a spacecraft driving its relative tangential velocity with respect to the docking port on the tumbling object to zero, essentially tracking the target's rotation and, at the same time, moving radially towards the docking port. However, space debris can have large sizes and high orbital spin rates. For example, as per [3], low Earth orbit expired satellites at altitudes greater than 500 km can have angular rates of up to 40 rpm. Also, a study on the attitude and spin period of the large out-of-service Envisat, using Satellite Laser Ranging, was conducted in [4], and for the satellite of dimensions 26 m $\times$ 10 m $\times$ 5 m, the tumbling period was found to be 134.74 s as of September 25, 2013. Adding to this, data on SpaceX's state-of-the-art Crew Dragon docking module from [5] suggests that during docking, sixteen Draco thrusters drive and orient the module towards the docking port, with each capable of providing the module a linear acceleration of 0.067 m/s^2. Thus, the limited thrust capabilities of service spacecrafts and the high acceleration requirements to track targets' angular motion can pose the restriction for motion in their close vicinity during the docking phase. The need for autonomous collision avoidance [6] in these scenarios is the inspiration for our work.

We utilize a framework for docking maneuvers called Lyapunov Vector Fields (LVF), which were first introduced for spacecraft maneuvers in [7], with the idea of superimposing artificial potential functions to a system state space for the system to follow a desired trajectory. An analytical guidance law based on this framework was used for spacecraft docking to a non-cooperative tumbling target in an elliptical orbit in [8] and further improved in [9]. The accuracy and the computationally lightweight nature of this guidance made it a more practical option than existing Model Predictive Control and Inverse Dynamics based approaches [10],[11] due to their high time spent for trajectory optimizations. However, none of these techniques presented a complete strategy for collision avoidance in close proximity to the docking port. In [8], a docking cone is utilized as a path constraint, but the body frame trajectory is planar, and it only considers a cross-section of the docking cone based on the chaser spacecraft's initial position. Close to the docking port, [9] too has a planar body frame trajectory based on unpredictable initial conditions. In [10], a collision avoidance algorithm for far-field rendezvous based on a rotating hyperplane was introduced, but generating this trajectory had the limitation of high computation times. In [11], a minimum separation constraint between the docking port and the target center of mass was added to an optimal control problem to prevent any contact between the chaser and the target surface. However, such a constraint would not be useful for large and irregular target geometries as the final position of the chaser would be far away from the docking port. In order to satisfy this constraint, there would also be a high computation time for optimization. In [12], a cissoid is defined within which the safe approach volume is confined. Still, the maneuver is assumed to be feasible only if the chaser starts from a point within the safety region. This scenario is highly unlikely in the case of a non-cooperative tumbling target.

This paper addresses collision avoidance by developing

[1]Research Intern, Department of Aerospace Engineering, Indian Institute of Science (IISc), CV Raman Road, Bengaluru, Karnataka 560012, India
[2]Doctoral Student, Department of Aerospace Engineering, IISc
[3]Professor, Robert Bosch Center for Cyber-Physical Systems and Department of Aerospace Engineering, IISc

Copyright ©2024 EUCA

a safety strategy during close proximity docking operations through an analytical guidance law using Lyapunov Vector Fields. It guarantees that no collisions will occur during docking, given a viable trajectory to a safe approach plane.

Our main contributions are,

1) Construction of a modified Lyapunov Vector Field for approaching a target spacecraft docking port along a collision-free plane.
2) Construction of a modified Cascaded Lyapunov Vector Field for entering the station-keeping phase of a docking maneuver along a collision-free plane.

The remainder of this paper is organized as follows: Section II reviews existing docking techniques using Lyapunov Vector Fields and highlights their limitations. Section III describes the modified vector field designs and how they overcome these limitations. Section IV proves the asymptotic stability of the new vector fields. Section V presents numerical simulation results, and Section VI concludes the paper with a discussion on the limitations of the proposed approach and possible future work.

II. AN OVERVIEW OF DOCKING MANEUVERS USING LYAPUNOV VECTOR FIELDS AND THEIR LIMITATIONS

In [8] and [9], both the chaser and the target move in elliptical orbits with J2 perturbed orbital dynamics, [13]. The target is provided with an initial angular velocity that does not need to be along a principal axis. It rotates without external torque acting on it, and a vector field is defined in its body-fixed frame. At close proximity to the target, the chaser tracks the target's rotation and orbital motion completely, so the body frame trajectory becomes significant. This section is an overview of existing guidance algorithms using Lyapunov Vector Fields (LVF), focusing on the target's body fixed frame. It also points out some limitations of existing methods.

A. Problem Formulation for Existing Techniques

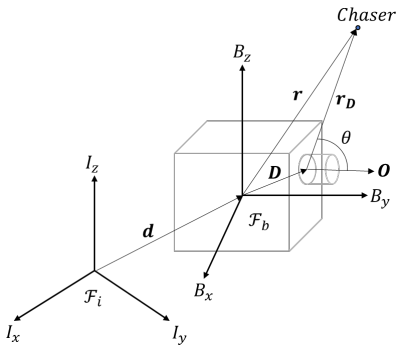

Fig. 1 Vectorial representation of chaser and target

Figure 1 depicts the instantaneous position of a chaser spacecraft, which is considered a point mass. A cube represents the target spacecraft in this figure for ease of visualization. The target's body-fixed frame, $\mathcal{F}_b$, is fixed to the target spacecraft with its origin at the target's center of mass and its coordinate axes pointing along the principal axes. The Earth-centered inertial reference frame $\mathcal{F}_i$ is the inertially stationary frame. The position of the origin of $\mathcal{F}_b$ with respect to the origin of $\mathcal{F}_i$ is given by vector $\mathbf{d} \in \mathbb{R}^3$.

The target's docking port position is given by vector $\mathbf{D} \in \mathbb{R}^3$ relative to the target center of mass. The unit vector $\mathbf{O} \in \mathbb{R}^3$ represents the orientation of the docking port in space. Vectors $\mathbf{r} \in \mathbb{R}^3$ and $\mathbf{r}_D \in \mathbb{R}^3$ denote the position of the chaser relative to the target center of mass and the docking port respectively, and $\theta \in \mathbb{R}$ is defined as the angle between $\mathbf{r}_D$ and $\mathbf{O}$.

The objective of the chaser is to approach the docking port with its relative velocity in the direction of $\mathbf{O}$ while both the chaser and the target are in orbit.

B. LVF Based Guidance [8]

In this approach, a Lyapunov potential function is given by $V = \mathbf{r}_D^T \mathbf{r}_D$, with the vector field that maps each point in space to a velocity vector chosen as

$$\mathbf{h}(\mathbf{r}_D) = v(\mathbf{r}_D)\left(\hat{\mathbf{C}}\cos\theta_N + \hat{\mathbf{S}}\sin\theta_N\right) \tag{1}$$

where $\hat{\mathbf{C}}$ and $\hat{\mathbf{S}}$ are unit vectors representing the contraction and circulation components, respectively, and $v(\mathbf{r}_D)$ is a speed term.

The contraction term is chosen to direct the chaser along the gradient of the potential function, and the circulation term is selected such that the chaser circles around the target in a plane made by the initial position vector $\mathbf{r}_{D(initial)}$ and $\mathbf{O}$.

A docking cone is used as a path constraint to prevent the chaser from making contact with the target's frame. A normalized angle measurement θ_N is used to help obey the docking cone angle constraint.

The resulting trajectory is circular until the chaser reaches the docking cone, followed by a combination of circular and radial contraction after entering this region.

C. Cascaded LVF Based Guidance [9]

Here, unlike LVF-based guidance, bounded acceleration to the chaser spacecraft is guaranteed for any initial distance from the target.

The docking maneuver is divided into 2 phases: a station-keeping phase followed by a contact phase. The station-keeping guidance is designed using two vector fields, one for radial contraction, which is active from the chaser start position, and the other for angular contraction, which is fully activated when the chaser reaches a defined radial distance α from the docking port. On reaching that distance, the chaser completely tracks the target's rotation inertially, making both vector fields non-time-varying in $\mathcal{F}_b$. We refer to this portion of the maneuver as the terminal docking phase.

During this period, the guidance equation in $\mathcal{F}_b$ is given by

$$\mathbf{h}(\mathbf{r}_D) = s_a(r_D, \theta)\hat{\mathbf{a}} \tag{2}$$

where $\hat{\mathbf{a}}$ is the angular contraction unit vector pointing along the gradient of the Lyapunov function, V_a.

The term $s_a(r_D, \theta)$ denotes the angular contraction speed. The resulting trajectory is circular along the plane formed by the $\mathbf{r}_D$ at the instant complete rotation tracking occurs, and $\mathbf{O}$. LVF-based guidance is used for the contact phase.

D. Limitations of Existing Techniques

Let a sphere of radius α centered at the target be referred to as the *tracking sphere*. For a collision-free chaser trajectory using the Cascaded LVF technique, this sphere must encompass the extended target (extended to account for the chaser's dimensions).

But the variation of inertial thrust produced with time using the Cascaded LVF Phase 1 guidance, as shown in Figure 2, reflects the high peak thrust the chaser would have to produce during the maneuver for tracking the target's rotation at large separations and high angular velocities. The angular velocities and dimensions considered in the plot are shown in Table I and are well aligned with the findings of [3] and [4]. The required thrust acceleration is up to ten times the limits from [5], which can risk thruster saturation of the chaser spacecraft and constrain the tracking sphere not to encompass the entire extended target. In this case, collision avoidance is needed while maneuvering on the tracking sphere.

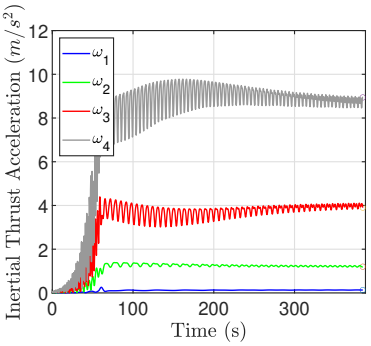

Fig. 2 Chaser- target separation of 18 m maintained during station keeping ($\alpha = 18$ m)

TABLE I Chaser and target initial conditions in $\mathcal{F}_b$

Target	
$\boldsymbol{\omega_1}^T$ (deg/s)	$\begin{pmatrix}1.0 & -2.4 & 4\end{pmatrix}$
$\boldsymbol{\omega_2}, \boldsymbol{\omega_3}, \boldsymbol{\omega_4}$	$3\boldsymbol{\omega_1}, 5.5\boldsymbol{\omega_1}, 8\boldsymbol{\omega_1}$
$J[Diag]$ (Kg.m^2)	$\begin{pmatrix}10 & 20 & 50\end{pmatrix}$
Chaser	
$\mathbf{r}^T_{D(initial)}$ (m)	$\begin{pmatrix}-100.0 & -100.0 & 0.0\end{pmatrix}$

In addition, there does not exist a method to optimize the CLVF speed parameters to accurately decide the position of the chaser at the beginning of the terminal phase. There is thus an uncertain initial position for the chaser in the target body frame at the beginning of the terminal docking phase.

In both the existing guidance techniques [8] and [9], the motion of the chaser spacecraft is planar in $\mathcal{F}_b$ when the target's rotation is fully tracked. However, due to the uncertainty in the chaser's initial position, its motion plane could pass through an appendage, blocking the docking port and leading to a collision.

III. PROPOSED GUIDANCE LAWS

The proposed Modified LVF and CLVF guidance laws address the drawbacks described by ensuring that the chaser approaches the docking port along a collision-free plane in $\mathcal{F}_b$. This is achieved by adding a third component of motion for the chaser away from the initial motion plane towards a safe approach plane.

A. Problem Formulation for Modified Vector Fields

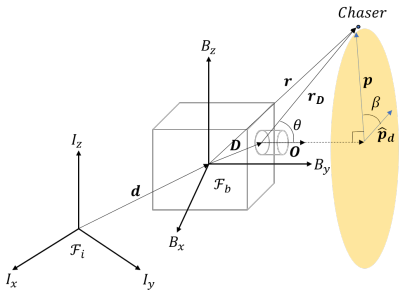

Fig. 3 Vectorial representation of chaser and target

Let vector $\mathbf{p} \in \mathbb{R}^3$ denote the projection of vector $\mathbf{r}_D$ onto a plane perpendicular to $\mathbf{O}$. This plane is shown in figure 3.

$$\mathbf{p} = \mathbf{r}_D - (r_D \cos\theta)\mathbf{O} \tag{3}$$

where $\mathbf{p}$, $\mathbf{O}$, and $\mathbf{r}_D$ lie on the same plane, which will be referred to as the *approach plane*. Let $\hat{\mathbf{p}}_d \in \mathbb{R}^3$ denote a unit vector lying on the plane perpendicular to $\mathbf{O}$. It denotes the desired approach direction. Vector $\mathbf{p}$ makes an angle β with $\hat{\mathbf{p}}_d$.

$$\cos\beta = \frac{\mathbf{p} \cdot \hat{\mathbf{p}}_d}{p} \tag{4}$$

Let the plane formed by vectors $\hat{\mathbf{p}}_d$ and $\mathbf{O}$ be the desired approach plane.

B. Modified LVF

The modified LVF guarantees a contraction in β before enforcing any motion towards the docking port, ensuring that the chaser would approach the docking port in close vicinity to the desired approach plane. The guidance command is given as

$$\mathbf{h}(\mathbf{r}_D) = v(\mathbf{r}_D)\left\{\left(\hat{\mathbf{C}}\cos\theta_N + \hat{\mathbf{S}}\sin\theta_N\right)\cos\beta_N + \hat{\mathbf{T}}\sin\beta_N\right\} \tag{5}$$

where $\hat{\mathbf{T}}$ denotes the *orientation component* directed perpendicular to the instantaneous approach plane, in the direction that reduces β fastest.

$$\hat{\mathbf{T}} = \frac{\mathbf{p} \times \hat{\mathbf{p}}_d \times \mathbf{p}}{\|\mathbf{p} \times \hat{\mathbf{p}}_d \times \mathbf{p}\|} \tag{6}$$

We define β_N as a normalized angle measurement, which helps ensure that the chaser starts contracting or circulating

only when $\beta \leq \beta_D$. Physically, $\beta \leq \beta_D$ denotes a safety region within which the chaser can move collision-free.

$$\beta_N = \begin{cases} \frac{\pi\beta}{2\beta_D} & \text{for } \beta \leq \beta_D \\ \frac{\pi}{2} & \text{otherwise} \end{cases} \tag{7}$$

C. Modified CLVF

The modified CLVF, in a similar way, guarantees a contraction in β before enforcing any circulation towards the station-keeping location vertically above the docking port. The guidance command is given as

$$\mathbf{h}(\mathbf{r}_D) = s_a(r, \theta, \beta)\hat{\mathbf{a}} + p_c(r, \beta)\hat{\mathbf{T}} \tag{8}$$

$$\hat{\mathbf{T}} = \frac{\mathbf{p} \times \hat{\mathbf{p}}_d \times \mathbf{p}}{\|\mathbf{p} \times \hat{\mathbf{p}}_d \times \mathbf{p}\|} \tag{9}$$

$$\beta_N = \begin{cases} \frac{\pi\beta}{2\beta_D} & \text{for } \beta \leq \beta_D \\ \frac{\pi}{2} & \text{otherwise} \end{cases} \tag{10}$$

With the modified $s_a(r_D, \theta, \beta)$ given by,

$$s_a(r_D, \theta, \beta) = \begin{cases} k_a \left(\frac{r_D}{\alpha}\right) \sin\theta \cos\beta_N & r_D > \alpha \\ k_a \left(\frac{\alpha}{r_D}\right) \sin\theta \cos\beta_N & \text{otherwise} \end{cases} \tag{11}$$

The magnitude term for the orientation component $\hat{\mathbf{T}}$ with k_t as a speed parameter is given by,

$$p_c(r_D, \beta) = \begin{cases} k_t \left(\frac{r_D}{\alpha}\right) \sin\beta & r_D > \alpha \\ k_t \left(\frac{\alpha}{r_D}\right) \sin\beta & \text{otherwise} \end{cases} \tag{12}$$

IV. STABILITY ANALYSIS

A. Stability of Modified LVF

Theorem 1: The Modified LVF guidance law given by Eqn. (5) is asymptotically stable at $\mathbf{r}_D = 0$ for $\theta \in [0, \theta_D]$ and $\beta \in [0, \beta_D]$.

Proof: For $V = \mathbf{r}_D^T \mathbf{r}_D$, taking the time derivative and assuming perfect tracking,

$$\dot{V} = \frac{\partial V}{\partial \mathbf{r}_D} \mathbf{h}(\mathbf{r}_D) \tag{13}$$

Since $\hat{\mathbf{S}}$ and $\hat{\mathbf{T}}$ are perpendicular to $\mathbf{r}_D$,

$$\dot{V} = -v_{max} \frac{r_D^4}{r_{D(initial)}^2} \cos\theta_N \cos\beta_N \tag{14}$$

For $\theta \in [0, \theta_D]$ and $\beta \in [0, \beta_D]$, $\cos\theta_N > 0$ and $\cos\beta_N > 0$. Therefore $\dot{V} < 0 \; \forall \; \mathbf{r}_D \neq 0$.

■

Theorem 2: Trajectories beginning at $\theta \in [\theta_D, \pi)$ and $\mathbf{r}_D \neq 0$ eventually enter $\theta < \theta_D$ for $\beta \in [0, \beta_D]$.

Proof: Let $V_\theta = \theta$. On differentiating,

$$\dot{V}_\theta = \frac{\mathrm{d}V_\theta}{\mathrm{d}\theta} \dot{\theta} \tag{15}$$

$$\dot{V} = -\left(\frac{v(\mathbf{r}_D) \sin\theta \cos\beta_N}{r_D}\right) \tag{16}$$

For $\theta \in [\theta_D, \pi)$, $\sin\theta > 0$. Also for $\beta \in [0, \beta_D]$, $\cos\beta_N > 0$. Therefore, $\dot{V}_\theta < 0$ proving that θ eventually becomes $< \theta_D$.

When $\theta = \pi$, $\hat{\mathbf{S}} = 0$, so θ would stay constant. Choosing $\hat{\mathbf{S}} = \hat{\mathbf{p}}_d$ is suitable at this condition as $\beta = 0$

■

Theorem 3: Trajectories beginning at $\beta \in [\beta_D, \pi)$ and $\mathbf{r}_D \neq 0$ eventually enter $\beta < \beta_D$ for any $\theta \in (0, \pi)$.

Proof: Let $V_\beta = \beta$

$$\dot{V}_\beta = \frac{\mathrm{d}V_\beta}{\mathrm{d}\beta} \dot{\beta} \tag{17}$$

$$\dot{V} = -\left(\frac{v(\mathbf{r}_D) \sin\beta}{r_D \sin\theta}\right) \tag{18}$$

For $\beta \in [\beta_D, \pi)$, $\sin\beta > 0$. Therefore, $\dot{V}_\beta < 0$, proving that β eventually becomes $< \beta_D$.

When $\beta = \pi$, $\hat{\mathbf{T}} = 0$, so β would stay constant. Choosing $\hat{\mathbf{T}} = \mathbf{O} \times \hat{\mathbf{p}}$ is suitable at this condition because β can be reduced in either direction. When $\theta = 0$, setting $\beta = 0$ is suitable as no change in β is required.

■

B. Stability of Modified CLVF

In Sections II-C and III-C, the guidance equations for the terminal portion of the maneuver were described. However, to prove the global stability of the modified CLVF guidance, its complete equation is used. This is given by,

$$\mathbf{h}(\mathbf{r}_D) = v_c(r)\hat{\mathbf{c}} + s_a(r, \theta, \beta)\hat{\mathbf{a}} + p_c(r, \beta)\hat{\mathbf{T}} + g(r)\boldsymbol{\omega}_{BI} \times \mathbf{r}_D \tag{19}$$

where $v_c(r)\hat{\mathbf{c}}$ and $g(r)\boldsymbol{\omega}_{BI} \times \mathbf{r}_D$ are identical to the terms used in [9]. The radial contraction unit vector pointing along the gradient of the Lyapunov function, V_c, is $\hat{\mathbf{c}}$. The radial speed is controlled by $v_c(r)$. The extent of rotation tracking is controlled by $g(r)$.

The field responsible for angular and orientation contraction here is initially time-varying in $\mathcal{F}_b$ due to partial rotation tracking and becomes fixed with time as the chaser reaches a distance α from the docking port. The radial field's attractor is a sphere of radius α centered at the docking port. Therefore, it is invariant to target rotation.

Theorem 4: Under the Modified CLVF guidance law given by Eqn. (19), $\mathbf{r}_D$ is globally asymptotically stable at the sphere centered at $\mathbf{D}$ and radius α, which is the attractor of the Lyapunov function V_c.

Proof: Taking first time derivative of V_c with respect to the inertial frame,

$$\dot{V}_c = \frac{\partial V_c}{\partial \mathbf{r}_D} \dot{\mathbf{r}}_D = \frac{\partial V_c}{\partial \mathbf{r}_D} \left(\dot{\mathbf{r}}_{inertial} - \dot{\mathbf{D}} - \dot{\mathbf{d}}\right) \tag{20}$$

$$\dot{V}_c = \frac{\partial V_c}{\partial \mathbf{r}_D}\mathbf{h}(\mathbf{r}_D) \tag{21}$$

Here, $\hat{\mathbf{a}}$, $\hat{\mathbf{T}}$ and $\boldsymbol{\omega}_{BI} \times \mathbf{r}_D$ are perpendicular to $\mathbf{r}_D$. Therefore,

$$\dot{V}_c = v_c r_D \tag{22}$$

Here, $v_c < 0$ for $r_D > \alpha$, and $v_c > 0$ for $r_D < \alpha$. Therefore, $\dot{V}_c < 0$ for $\alpha \neq 0$, completing the proof.

■

Theorem 5: Under the Modified CLVF guidance law given by Eqn. (19), provided $\beta \in [0, \beta_D]$, vector $\mathbf{r}_D$ is asymptotically stable at $\theta = 0$, which is the attractor of the Lyapunov function V_a.

Proof: Taking first derivative of V_a,

$$\dot{V}_a = \frac{\mathrm{d}V_a}{\mathrm{d}\theta}\dot{\theta} \tag{23}$$

$$\dot{V}_a = \frac{\mathrm{d}V_a}{\mathrm{d}\theta}\left(-\frac{s_a}{r_D} + (1-g)\mathbf{O}\cdot(\boldsymbol{\omega}_{BI} \times \mathbf{r}_D)\right) \tag{24}$$

Theorem 4 mandates that r_D converges to α. And at $r_D = \alpha$, $g(r) = 1$ reducing the equation to,

$$\dot{V}_a = \frac{\mathrm{d}V_a}{\mathrm{d}\theta}\left(-k_a \frac{\sin\theta \cos\beta_N}{\alpha}\right) \tag{25}$$

For $\beta \in [0, \beta_D]$, $\cos\beta_N > 0$, and $\frac{\mathrm{d}V_a}{\mathrm{d}\theta} > 0$ as it is required that $V_a = 0$ at $\theta = 0$ and V_a increases as θ increases. Therefore, on reaching the attractor of V_c, $\dot{V}_a < 0$, thus completing the proof.

When $\theta = \pi$, $\hat{\mathbf{a}} = 0$, so θ would stay constant. Choosing $\hat{\mathbf{a}} = \hat{\mathbf{p}}_d$ is suitable at this condition as $\beta = 0$

■

Theorem 6: Trajectories beginning at $\beta \in [\beta_D, \pi)$ and $\mathbf{r}_D \neq 0$ eventually enter $\beta < \beta_D$ for any $\theta \in (0, \pi)$.

Proof: Following Theorem 3 and using Theorem 4,

$$\dot{V} = -\left(\frac{p_c \sin\beta}{r_D \sin\theta}\right) \tag{26}$$

For $\beta \in [\beta_D, \pi)$, $\sin\beta > 0$. Therefore, $\dot{V}_\beta < 0$ proving that β eventually becomes $< \beta_D$.

■

V. DESIGN OF DOCKING MANEUVER

The proposed docking maneuver is carried out in two phases, using the modified CLVF in Phase 1, followed by the modified LVF in Phase 2.

Simulations are performed in the inertial frame $\mathcal{F}_i$. However, the design example in this paper compares the terminal portion of the existing and modified maneuvers by viewing trajectories in the target's body-fixed frame $\mathcal{F}_b$, as collisions with appendages fixed to the target's body depend on the chaser's motion in $\mathcal{F}_b$. The satellite model used for the design example is obtained from [14]. Videos of the simulations are linked in the figure captions. The initial conditions are shown in Table II,

TABLE II Chaser and target initial conditions in $\mathcal{F}_b$

Target	
$\mathbf{D}^T$ (m)	$(0.0 \quad 0.0 \quad 1.4)$
$\mathbf{O}^T$, $\hat{\mathbf{p}}_d^T$	$(0.0 \quad 0.0 \quad 1.0)$, $(-1.0 \quad 0.0 \quad 0.0)$
θ_D, β_D (deg)	12, 20
α (m)	7.070
Chaser	
$\mathbf{r}^T_{(Phase\ 1)}(m)$	$(0.0 \quad -6.0 \quad -6.0)$
$\mathbf{r}^T_{(Phase\ 2)}(m)$	$(0.0 \quad -1.75 \quad 9.0)$

A. Phase 1: Station Keeping

Here, some approach trajectories to the station keeping position vertically above the docking port are obstructed by solar panels. An obstructed plane intersecting the solar panels is red, and a safe plane that does not intersect any such appendage is cyan. Figure 4 shows a scenario where the chaser's initial position is on the obstructed plane, and CLVF-based guidance is applied. The resulting planar trajectory causes the chaser to collide with a solar panel. In Figure 5, the modified CLVF-based guidance is applied with the same initial conditions, where the chaser orients itself to the safe approach plane before circulating towards the station-keeping position, therefore avoiding contact with the solar panels.

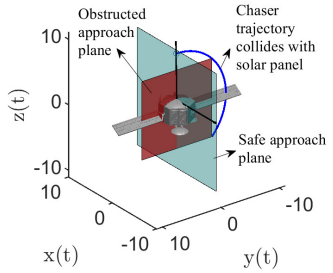

Fig. 4 Cascaded LVF trajectory lies on an obstructed approach plane (`https://bit.ly/46YS5Jv`)

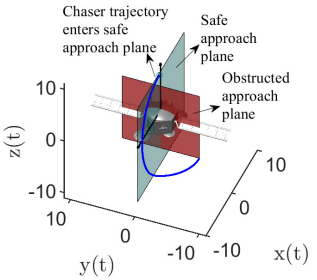

Fig. 5 Obstructed solar panels avoided by approaching along the safe approach plane (`https://bit.ly/3MUH8Rx`)

B. Phase 2: Contact

Ideally, the chaser should be vertically above the docking port at the end of Phase 1, so Phase 2 would just be linear motion along the line of intersection of the safe and

obstructed planes. However, under the occurrence of any tracking error during Phase 1 due to disturbances such as sensor noise, the chaser's position might not end up vertically above the docking port, and it could lie on an obstructed plane at the beginning of Phase 2. In such a scenario, if the chaser carried out Phase 2 using LVF-based guidance as shown in Figure 6, its trajectory would entirely lie on the obstructed plane till it converges to the docking port. This would pose a high risk of collision while the chaser is outside the docking cone. This limitation is overcome using the modified LVF-based guidance by making the chaser return to a safe approach plane and spending most of its trajectory in close vicinity to the safe approach plane, as shown in Figure 7, therefore reducing the probability of collision, and at the same time providing robustness to the guidance law by mitigating the tracking error.

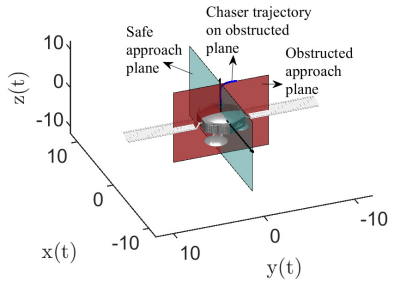

Fig. 6 Approach from obstructed approach plane, risking collisions (`http://bit.ly/47nLaJG`)

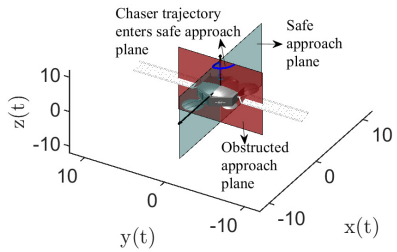

Fig. 7 Tracking error eliminated by returning to safe approach plane (`https://bit.ly/3FLBeOi`)

VI. CONCLUDING REMARKS

The modified guidance law provides a level of obstacle avoidance to body-fixed appendages on a tumbling target without compromising on the computational lightness of the initial algorithm. This is achieved by designing a 3D vector field that satisfies an approach plane constraint. The modified equations have the same structure and therefore can be plugged back into the inertial frame acceleration equations, retaining the advantages of earlier works. Some issues with the proposed methods that can lead to interesting future work are the following,

The proposed guidance law is useful when the chaser has to track the target's rotation within a sphere encompassing the boundaries of the extended target. However, it does not provide a strategy for the chaser to enter this sphere in a collision-free path or to reach the safe approach plane outside the sphere. Another issue is that a collision-free path must exist for the chaser while orienting itself to the safe approach plane. This can be satisfied by appropriately deciding the safe approach plane. It would be useful to develop a guidance strategy that accounts for a scenario where there is no available path to the safe approach plane from the chaser's position.

We point out that these limitations also exist in the existing work in literature but can be addressed using our proposed framework.

REFERENCES

[1] D. J. Kessler and B. G. Cour-Palais, "Collision frequency of artificial satellites: The creation of a debris belt," *Journal of Geophysical Research: Space Physics*, vol. 83, no. A6, pp. 2637–2646, 1978.

[2] K. Wormnes, R. Le Letty, L. Summerer, R. Schonenborg, O. Dubois-Matra, E. Luraschi, A. Cropp, H. Krag, and J. Delaval, "ESA technologies for space debris remediation," in *6th European Conference on Space Debris*, vol. 1, pp. 1–8, ESA Communications ESTEC Noordwijk, The Netherlands, 2013.

[3] M. Kaplan, B. Boone, R. Brown, T. Criss, and E. Tunstel, "Engineering issues for all major modes of in situ space debris capture," in *AIAA Space Conference & Exposition*, p. 8863, 2010.

[4] D. Kucharski, G. Kirchner, F. Koidl, C. Fan, R. Carman, C. Moore, A. Dmytrotsa, M. Ploner, G. Bianco, M. Medvedskij, *et al.*, "Attitude and spin period of space debris Envisat measured by satellite laser ranging," *IEEE Transactions on Geoscience and Remote Sensing*, vol. 52, no. 12, pp. 7651–7657, 2014.

[5] "SpaceX." `https://www.spacex.com/vehicles/dragon/`, 2023. Accessed on October 31 2023.

[6] J. A. Starek, B. Açıkmeşe, I. A. Nesnas, and M. Pavone, "Spacecraft autonomy challenges for next-generation space missions," in *Advances in Control System Technology for Aerospace Applications*, pp. 1–48, Springer, 2015.

[7] I. Lopez and C. R. Mclnnes, "Autonomous rendezvous using artificial potential function guidance," *Journal of Guidance, Control, and Dynamics*, vol. 18, no. 2, pp. 237–241, 1995.

[8] J. G. Hough and S. Ulrich, "Lyapunov vector fields for thrust-limited spacecraft docking with an elliptically-orbiting uncooperative tumbling target," in *AIAA Scitech 2020 Forum*, p. 2078, 2020.

[9] J. G. W. Hough, *Cascaded Lyapunov Vector Fields for Spacecraft Relative Trajectory Tracking in Rotating Reference Frames Under Acceleration Constraints*. PhD thesis, Carleton University, 2021.

[10] A. Weiss, M. Baldwin, R. S. Erwin, and I. Kolmanovsky, "Model predictive control for spacecraft rendezvous and docking: Strategies for handling constraints and case studies," *IEEE Transactions on Control Systems Technology*, vol. 23, no. 4, pp. 1638–1647, 2015.

[11] J. Ventura, M. Ciarcia, M. Romano, and U. Walter, "An inverse dynamics-based trajectory planner for autonomous docking to a tumbling target," in *AIAA Guidance, Navigation, and Control conference*, p. 0876, 2016.

[12] X. Li, Z. Zhu, and S. Song, "Non-cooperative autonomous rendezvous and docking using artificial potentials and sliding mode control," *Proceedings of the Institution of Mechanical Engineers, Part G: Journal of Aerospace Engineering*, vol. 233, no. 4, pp. 1171–1184, 2019.

[13] H. D. Curtis, *Orbital Mechanics for Engineering Students*. Butterworth-Heinemann, 2013.

[14] "Free CAD Designs, Files 3D models | the GrabCAD Community Library." `https://grabcad.com/library/satellite-2`, November 2013. Accessed on October 31 2023.